Materials Today Bio 28 (2024) 101233

Contents lists available at ScienceDirect

Materials Today Bio

journal homepage: www.journals.elsevier.com/materials-today-bio

A wireless, battery-free device for electrical neuromodulation of bladder contractions

Jun Li [a,d], Guoxian Deng [b], Xianping Li [b], Lingxuan Yin [c], Chunhui Yuan [b], Wei Shao [c], Xiaowen Xia [b], Junan Yan [a,b,d,**], Jiwei Yao [b,e,*]

[a] School of Physical Science and Technology, Guangxi University, Nanning, 530004, China
[b] Department of Urology, PLA Naval Medical Center, Naval Medical University, Shanghai, 200052, China
[c] Guangxi Key Laboratory of Special Biomedicine, School of Medicine, Guangxi University, Nanning, 530004, China
[d] Department of Urology, Southwest Hospital, Third Military Medical University, Chongqing, 400038, China
[e] Center for Neurointelligence, School of Medicine, Chongqing University, Chongqing, 400030, China

ARTICLE INFO

Keywords:
Electrical neurostimulation
Wireless device
Major pelvic ganglion
Bladder
Urodynamics
Urination control

ABSTRACT

Lower urinary tract dysfunction (LUTD) is a prevalent condition characterized by symptoms such as urinary frequency, urgency, incontinence, and difficulty in urination, which can significantly impair patient's quality of life and lead to severe physiological complications. Despite the availability of diverse treatment options, including pharmaceutical and behavioral therapies, these approaches are not without challenges. The objective of this study was to enhance treatment options for LUTD by developing a wireless, battery-free device for managing bladder contractions. We designed and validated a compact, fully implantable, battery-free pulse generator using the magnetic induction coupling mechanism of wireless power transmission. Weighing less than 0.2 g and with a volume of less than 0.1 cubic centimeters, this device enables precise stimulation of muscles or neurons at voltages ranging from 0 to 10 V. Wireless technology allows real-time adjustment of key stimulation parameters such as voltage, duration, frequency, pulse width, and pulse interval. Our findings demonstrate that the device effectively controlled bladder contractions in mice when used to stimulate the Major Pelvic Ganglion (MPG). Additionally, the device successfully managed micturition in mice with bilateral transection of the pudendal nerve. In conclusion, the development of this innovative wireless pulse generator provides a safer and more cost-effective alternative to conventional battery-powered neurostimulators for bladder control, addressing the limitations of such devices. We anticipate that this novel technology will play a pivotal role in the future of electrical stimulation therapies for voiding dysfunctions.

1. Introduction

The lower urinary tract plays an essential role in the storage and regular elimination of urine[1–5]. However, lower urinary tract dysfunction (LUTD), characterized by symptoms such as urinary frequency, urgency, incontinence, and difficulty in urination, not only severely impacts patients' daily life and social activities but also may lead to a series of more serious physiological complications [6,7]. Chronic voiding disorders can result in an overactive bladder, decreased bladder wall compliance, morphological changes, and upper urinary tract pathologies, such as ureteral reflux, hydronephrosis, and renal damage, potentially progressing to end-stage renal disease, which poses a threat to patients' lives [7,8]. Despite the availability of various treatment modalities for LUTD, including behavioral therapy and pharmacological interventions, these approaches still face numerous challenges [9]. For instance, in patients with refractory overactive bladder syndrome (OAB) [10,11], behavioral therapy may fail, and monotherapy with antimuscarinic agents like M-receptor antagonists may not achieve the desired efficacy after 6–12 weeks of treatment or may be associated with intolerable side effects [12]. Additionally, neurogenic lower urinary tract dysfunction (NLUTD), such as that caused by incomplete spinal cord injury and multiple sclerosis (MS), presents even greater demands for existing treatment options [13,14]. Among these challenging cases, neuromodulation therapy, particularly

* Corresponding author. Department of Urology, PLA Naval Medical Center, Naval Medical University, Shanghai, 200052, China.
** Corresponding author. Department of Urology, PLA Naval Medical Center, Naval Medical University, Shanghai, 200052, China.
E-mail addresses: junan_yan@aliyun.com (J. Yan), moerfusi@126.com (J. Yao).

https://doi.org/10.1016/j.mtbio.2024.101233
Received 30 May 2024; Received in revised form 4 September 2024; Accepted 7 September 2024
Available online 13 September 2024

sacral neuromodulation (SNM), offers renewed hope owing to its adjustable and reversible stimulation properties [15,16]. SNM has become a well-established therapy for refractory non-neurogenic LUTD [17].

SNM delivers electrical currents to nerves or tissues via external or implanted electrodes to modulate neural activity or facilitate tissue repair. Since the U.S. Food and Drug Administration (FDA) approved SNM for the treatment of urge incontinence in 1997, its indications have expanded to include the treatment of frequency-urgency syndrome and non-obstructive urinary retention[17–19]. Several brands currently offer SNM systems, such as Medtronic, Boston Scientific, Prometheus, NuVetra, and Axonics, each providing different electrode and pulse generator (stimulator) configurations [18]. However, the Medtronic Intellis™ System is acknowledged as one of the smallest neural stimulators on a global scale, its weight remains above the 10-g threshold [18]. Despite its compact size, the system is not without risks, as it is still susceptible to post-implantation complications such as infection or device displacement. In addition, the relatively high cost associated with its treatment may impose financial constraints that limit its accessibility to certain patient populations. While addressing these challenges, current research aims to reduce stimulator size, minimize post-implantation infection and displacement risks, and improve patient acceptance. Wireless systems that use near-field energy transfer are considered potential solutions to these issues. Wireless and battery-free systems eliminate the need for frequent maintenance and potential discomfort caused by wired connections, thus enhancing patient compliance and continuous monitoring capabilities[20–30]. Recent reports indicate that soft wireless implants can achieve long-term monitoring and interventions in the body without requiring batteries or external connections[31–35]. Furthermore, Jang et al. have successfully controlled micturition by directly targeting the bladder using an optogenetic wireless system [32,36]. Additionally, a fully implanted, battery-free, high-power platform has been utilized in research on chronic spinal and muscular functional electrical stimulation [37]. Lee et al. suggested that implantable electronics with a flexible neural clip interface could effectively treat underactive bladder (UAB) syndrome [38]. Moreover, Lee et al. have demonstrated the control of micturition through direct electrical stimulation of the bladder wall using a wireless, fully implantable electronic complex [39]. These findings highlight the potential of flexible wearable electronics in regulating bladder function.

In this study, we designed and validated a miniature, fully implantable, battery-free wireless stimulator based on the theory of wireless power supply using magnetic induction coupling. This wireless stimulator, weighing less than 0.2 g and with a volume of less than 0.1 cubic centimeters, enables precise stimulation of peripheral nerves or muscles at 0–10 V. The device allows for real-time adjustment of key parameters, such as stimulation voltage, duration, frequency, pulse width, and pulse interval via wireless technology. This device was used to stimulate the Major Pelvic Ganglion (MPG) to control bladder contractions in mice. Additionally, after bilateral pudendal nerve transection, this device effectively managed micturition in mice. In conclusion, the development of this wireless stimulator resolves the limitations associated with traditional battery-powered electrical stimulators for bladder control and offers a safer and more cost-effective treatment alternative. We anticipate that this innovative device will play a pivotal role in the future of electrical stimulation treatment of voiding dysfunction.

2. Methods

2.1. Device fabrication and encapsulation

The copper microcircuit of the device was created by etching a 35 μm-thick copper foil. An appropriate amount of lead-free solder paste No. 9 was applied to the designated component soldering positions on the microcircuit, followed by sequential placement of capacitors, Schottky diodes, and microscale inorganic light-emitting diode (μ-ILED) indicators. The microcircuit was then moved to a constant-temperature soldering station at 200°C for a 10-s soldering process. After soldering, the device was placed on a glass slide measuring 15 × 50 × 1 mm for encapsulation. Polydimethylsiloxane (PDMS) was spin-coated at 1000 rpm for 30 s and cured at 70°C for 6 h to form a first layer with a thickness of 100 μm. The device with the first layer was flipped and encapsulated with PDMS again, spun at 1000 rpm for another 30 s, and cured at 70°C for 6 h to complete the second layer encapsulation.

2.2. Energy transmission device assembly

The radio frequency (RF) power transmission system consisted of the following components: a signal generator (N9310A, Agilent), a power amplifier (13.56 MHz RFPD), a direct current (DC) power supply with a heat sink (Keysight Technologies), and impedance-matched RF antennas. The power amplifier and fan were powered by separate DC power supplies. The signal input of the power amplifier was connected to the output of the signal generator, whereas the signal output of the power amplifier was connected to a circular copper tube antenna with a diameter of 20 cm and a characteristic impedance of 50 Ω. Together, these components form the RF energy emission field.

2.3. Device response frequency and system latency testing

Two 36-gauge American Wire Gauge (AWG) silver wire electrodes, each 10 cm in length, were soldered to the stimulation site of the device. The other ends of the silver wires were connected to the recording cable (Channel One) of a multichannel physiological recorder (RM6240E, Chengdu Instrument Factory, China). Concurrently, the modulation port of the RF power transmission system was connected to Channel Two for long-duration recording. The recorded data from Channel Two included information on the start time, duration, and cycle of the device's voltage output. The difference in time between the appearance of a marker on Channel Two and the start of the voltage change on Channel One represented the latency of the wireless stimulation system.

2.4. Device output voltage testing

Two 10-cm-long 36 AWG silver wire electrodes were soldered to the stimulation site of the device with the other ends connected to the voltage-measurement leads of a digital high-precision multimeter. Changes in the voltage output of the device at different RF power transmission levels were recorded using a voltage measurement function.

2.5. Animals

Wild-type (WT) C57BL/6J mice were housed under standard laboratory conditions with free access to food and water provided by the SPF (Beijing) Biotechnology Co., Ltd. All experimental procedures followed the Animal Welfare Guidelines of the Third Military Medical University (TMMU) and the National Institutes of Health Guidelines for the Care and Use of Laboratory Animals and were approved by the TMMU Animal Care and Use Committee. Mice of comparable age and weight were randomly assigned to control groups (laparotomy and sham groups) or the device-implanted group. The laparotomy (Lap) group consisted of mice that underwent surgery without device implantation. The sham group consisted of device-implanted mice without stimulation.

2.6. Cystometry

Cystometry was performed according to established procedures [2,40]. Male C57BL/6J mice were anesthetized with isoflurane (3% induction, 1.5% maintenance) and placed on a temperature-controlled pad in the supine position. An eye ointment Bepanthen® (Bayer) was used to protect the eyes. Following shaving of the abdominal fur, a 1 cm

midline incision was made to expose the bladder. A 7 cm long PE10 catheter was then carefully inserted into the bladder dome using a 20 G (0.9×80 TWLB) needle. The PE10 catheter was secured to the bladder dome with a 6-0 nonabsorbable suture, and the other end of the catheter was passed through the abdominal wall and exited from the dorsal neck skin. The connections were reinforced using Vetbond Tissue Adhesive (3M, 1469SB). Subsequently, mice received intraperitoneal (i.p.) injections of ketoprofen (5 mg/kg) and enrofloxacin (5 mg/kg) for postoperative care.

A multichannel physiological recording system (RM6240E, Chengdu Instrument Factory, China) was employed, with four channels connected to a pressure transducer (YPJ01H; Chengdu Instrument Factory, China). The pressure transducer system was attached to the PE10 catheter on the neck of the mouse. An infusion pump (RWD404; RWD Technology Corp., Ltd., China) was used to administer the infusions at rates ranging from 5 to 50 μl/min. The pressure recording parameters included a sensitivity of 12.5 cmH_2O, no high-pass filtering in hardware, and a low-pass filter set at 30 Hz. Post-recording analysis involved assessing peak pressure and pressure differentials. RM6240E's analysis tools were used for data extraction, which was then exported to Excel for further statistical analysis using SPSS 23 software (IBM, USA).

2.7. Device implantation surgery

Male C57BL/6J mice were anesthetized with isoflurane (3% induction, 1.5% maintenance) and placed on a temperature-controlled pad in the supine position. A 1-cm incision was made along the midline of the abdomen. The tissue around the prostate was bluntly dissected using forceps to facilitate the implantation of the nearby stimulation electrode. A 20-gauge needle was used to place the cuff electrode of the device over the major pelvic ganglion (MPG), typically located on the left side, and the four connection points of the electrode were secured with a 6-0 non-absorbable suture. The entire contact site was then fixed with Kwik-Sil silicone adhesive and 3M tissue glue. Abdominal muscles and skin were sutured separately using 5-0 sutures. At the end of surgery, the mice were intraperitoneally injected with ketoprofen (5 mg/kg, i.p.) and enrofloxacin (5 mg/kg, i.p.).

2.8. Hematoxylin&Eosin staining

Bladder tissues were stained using a Hematoxylin&Eosin (H&E) staining kit (R23261, Shanghai Saint-Bio Biotechnology Co., Ltd). The procedure is as follows: 5-μm thick bladder sections were fixed in paraformaldehyde for 3 min, followed by a 3-min water wash. Hematoxylin staining was performed for 1 min, followed by differentiation for 10 s, and a 1-min water wash. Sections were then blued in a bluing reagent for 2 min, and washed in water for 1 min. Eosin staining was applied for 30 s, followed by a 30-s water wash. The sections were dehydrated using a graded series of ethanol (95%-100%), cleared in xylene, and mounted with neutral resin. Images were captured at 20× and 40× magnification using a slide scanning system (PanoBrain, Meca Scientific).

2.9. Statistical analysis

The sample size was not determined by statistical methods. Normality of the data was assessed using the Shapiro-Wilk test and histograms in the SPSS23 software (IBM, USA) to check for normal distribution. All statistical analyses were two tailed. Paired and unpaired two-tailed Student's *t-tests* or *F-tests* were used for normally distributed data. The Wilcoxon and Mann-Whitney *U* test or Kruskal-Wallis test were used for non-normally distributed data. Statistical significance was set at $p < 0.1$. Values below this threshold were considered statistically significant and as indicated in the figures. *$P < 0.05$; **$P < 0.01$; ***$P < 0.001$; ns indicates no significant difference. Error bars represent mean ± standard error of the mean (s.e.m.) and reflect the average value and its precision. For data that do not follow a normal distribution, error bars representing the 5th to 95th percentiles show the range within which the central 90% of data points fall.

3. Results

3.1. Overview of wireless battery-free functional electrical stimulation device

We designed and fabricated a flexible, biocompatible, and wireless electrical stimulation device to minimize its size, measuring 1 cm × 1 cm in surface area, approximately 0.1 cm in height, and weighing approximately 0.2 g. This device, fully implantable into the subcutaneous area of a mouse's abdomen, enables electrical stimulation of peripheral nerves or muscles. Its battery-free design, coupled with flexible mechanics and a low displacement volume (0.1 cm^3), minimizes the impact on the animal's appearance and spontaneous exploratory activity (Fig. 1A-C). To further reduce the weight of the electrical stimulation device, wireless power transfer (WPT) functionality was integrated into a thin, flexible square printed circuit (FPC). A dual-loop receiving antenna for the device was formed via laser ablation on the top and bottom coils, thereby enabling a battery-free design. The device's electronic components-including a Schottky diode, capacitor for rectification, and a μ-ILED for local illumination-were soldered to the antenna, providing power supply and active control (Fig. 1A-D). Encapsulation was achieved using a bilayer film of poly (p-xylylene)-polydimethylsiloxane (PDMS) (20-200 μm), excluding the electrical stimulation contact point, to prevent inflammation and ensure soft contact with the surrounding tissues (Fig. 1A and 1D). The encapsulated electrical stimulation device was subcutaneously implanted in the abdomen to target abdominal nerves or muscle tissue for electrical stimulation (Fig. 1C). The unencapsulated electrical stimulation device features two exposed bare copper contacts that form the electrical stimulation interface, providing contact points for the electrical stimulation output (Fig. 1D and 1E). The snake-shaped extension at the front of the electrical stimulation interface can stretch up to 1.5 cm, enhancing flexibility for electrical stimulation localization during surgery (Fig. 1E). For secure fixation, the interface copper cover can be sutured, and a biocompatible tissue adhesive is used to wrap the stimulated nerve tissue, ensuring a stable connection between the electrical stimulation device and nerve (Fig. 1F). To enable wireless power supply for the electrical stimulation device, we developed a power transfer system (Fig. 1G-H). The system includes a radio frequency (RF) source for energy provision, employs magnetic coupling for power transmission, and facilitates energy collection using a wireless electrical stimulation device. The RF source energy supply uses a 13.56 MHz signal generator paired with a power amplifier to drive the primary single-loop RF transmission antenna for the wireless power supply.

3.2. Characterization of wireless electrical stimulation device

To test the energy-harvesting capability of the wireless electrical stimulation device, the device was placed at the center of the bottom area of a circular experimental cage (diameter 20 cm). When the primary single-loop RF antenna transmitted power in the range of 4 W to 12 W, the rectified voltage of the device varied from 0 V to 10 V (Fig. 2A). The transmission power of this primary single-loop RF antenna was adjustable and linearly correlated with the receiving power of the electrical stimulation device. The rectified current-voltage response (Supplementary Fig. 1a) and the rectified power transmission characteristics (Supplementary Fig. 1b) highlight the key operational features. This characteristic can be used to estimate the power requirements of the larger experimental chambers. The stimulation parameters of the electrical stimulation device were wirelessly transmitted through a custom protocol, controlling the amplitude, pulse width, period, and duration by adjusting the RF power, supporting a maximum of 1000 Hz

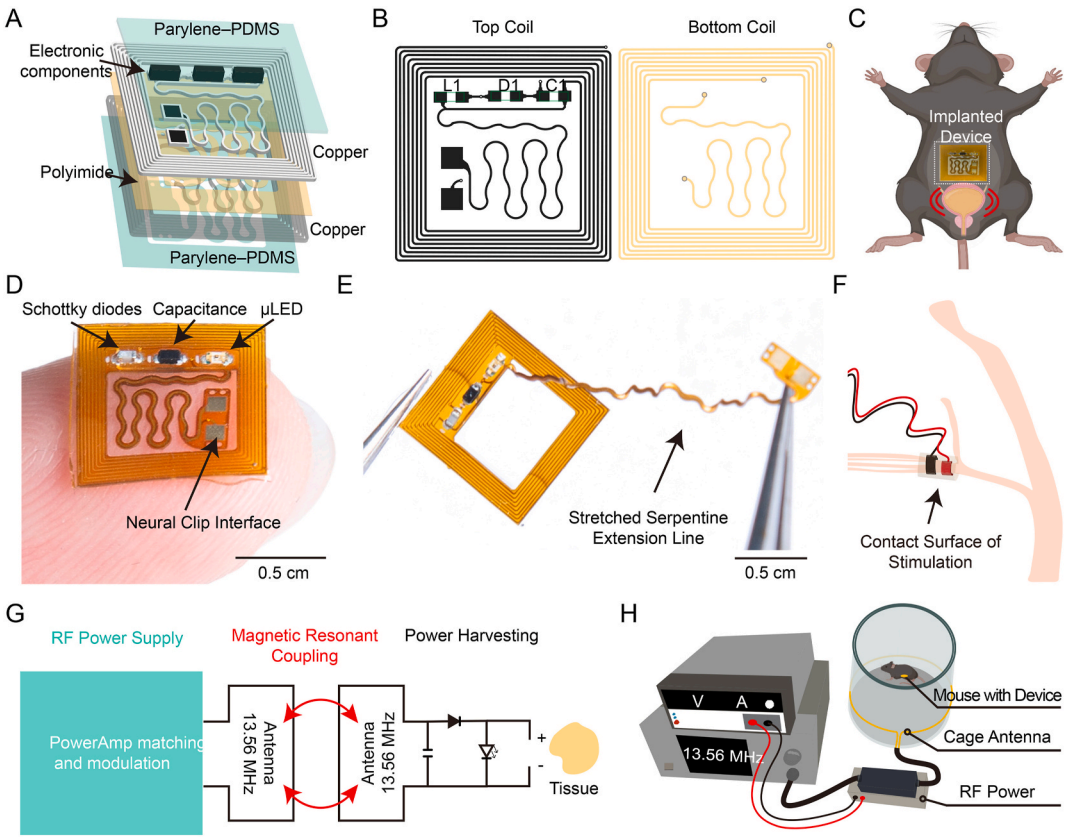

Fig. 1. Overview of Power Transmission Systems (A) Subcutaneous tissue device for non-tethered animal electrical stimulation research, featuring dynamically programmable operation. (B) Top and bottom coil design, enabling wireless power transfer and ensuring efficient energy reception and distribution. (C) Schematic of subcutaneous implantation location in the abdomen. (D) Photograph showcasing the electrical stimulation device's physical attributes and design features. (E) Photograph during implantation with the serpentine antenna stretched, highlighting device flexibility. (F) Schematic illustrating stimulation point fixation to tissue. (G) Platform frame supporting Near Field Communication (NFC) for independent and programmable control of power transmission and stimulation parameters. (H) Schematic of the platform for wireless power transmission, including a 13.56 MHz power source, power amplifier, and impedance-matching antenna, controlled via PC for transmission control.

and 1 ms pulse width stimulation (Fig. 2B). The stimulation parameters used in this study were as follows: total stimulation duration, 5 s; voltage amplitude, 1 V; frequency, 25 Hz; pulse width, 10 ms; and pulse interval, 30 ms (Fig. 2C). Next, we evaluated the effect of the newly designed device on the movement of the mice after implantation. According to our findings, there were no significant differences in the average total distance traveled, speed, and average number of movement circles of representative mice in an open field environment for 5 min between the laparotomy (Lap) group and the device-implanted (Dev) group without stimulation. This suggests that the effect of subcutaneous implantation on the movement behavior of mice was minimal (Fig. 2D–G).

Notably, previous studies have indicated that implants made from FPC and encapsulated in PDMS exhibit long lifespans and do not lead to erosion of the skin or muscle tissues in animals [31,33,34,41]. In this study, considering the heat generation when current flows through the conductor during device operation, efforts were made to minimize the temperature variation at the implantation site. During the design and manufacturing process, wire with a diameter supporting a maximum current of 100 mA was used. By reducing the current density, heat generation was minimized. At an output voltage of 1 V, the output current was 0.35 mA, and the maximum rectified current was 3.5 mA (Supplementary Fig. 1c). Furthermore, the change in surface temperature adjacent to the device was measured under different voltages, duty cycles, and prolonged operation. After operating for 10 min at 1 V, 25 Hz, and 100% duty cycle, the maximum surface temperature change was 0.2°C (Supplementary Fig. 1d). At 9 V (resistors replaced μ-ILED), 25 Hz, and 100% duty cycle, the maximum surface temperature change after 10 min was 0.1°C (Supplementary Fig. 1e). Under long-term operation at 1 V, 25 Hz, and 25% duty cycle, the maximum surface temperature change was 0.1°C (Supplementary Fig. 1f). Overall, the wireless electrical stimulation device demonstrated effective energy-harvesting capabilities, precise control of stimulation parameters, and minimal impact on mouse movement behavior and implantation site temperature, indicating its potential for safe and long-term biomedical applications.

3.3. *Application of wireless electrical stimulation device to control mouse bladder contraction*

Previous studies have shown that bladder emptying can be achieved by stimulating the sacral anterior/ventral roots that dominate the bladder muscle[42–44]. To evaluate the in vivo effects of the wireless device, we targeted the MPG, which is anatomically connected to the bladder and directly innervates the bladder muscle [45,46]. The wireless device was placed between the skin and abdominal muscles in male WT mice, with the stimulation contact point cuffing the MPG and secured with a Kwik-Sil silicone adhesive (Supplementary Fig. 3a). Subsequently, intravesical pressure (IVP) traces were monitored during wireless electrical stimulation using non-continuous transvesical infusion cystometry in urethane-anesthetized mice (Fig. 3A). Observations indicate that wireless electrical stimulation of the MPG (stimulation frequency: 25 Hz; duration: 5 s; pulse width: 10 ms; pulse interval: 30 ms) with stimulation voltage at 1 V resulted in immediate and time-locked increases in IVP. Furthermore, the effects of various

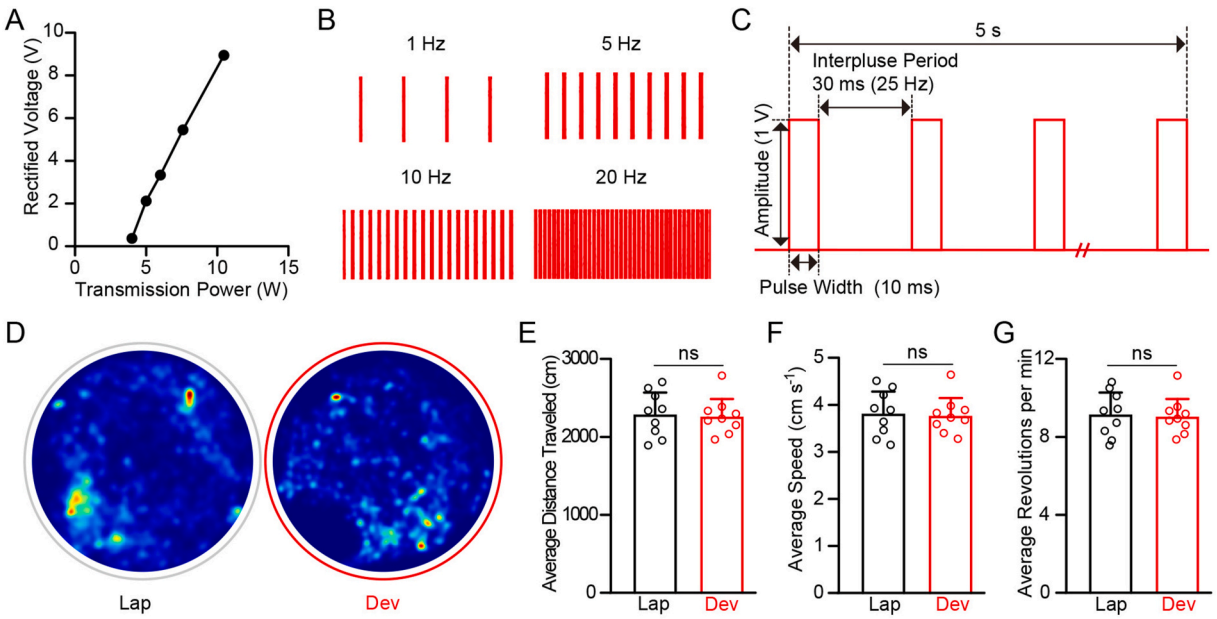

Fig. 2. Electrical Characteristics of the Electrical Stimulation Device and Its Effects on Animal Behavior (A) Relationship between platform power transmission and the device's voltage output. (B) Parameters for low-frequency stimulation operation of the device. (C) Stimulation parameter schematic, including total duration, voltage, frequency, pulse width, and interval. (D) Heat map showing mouse movement trajectories in an open field, comparing the laparotomy group (Lap) and the device-implanted (Dev) group without stimulation (observed for 5 min in a circular area). The Lap group consisted of mice that underwent surgery without device implantation. (E–G) Quantification of the total length of mouse movement trajectories, average movement speed, and average number of movement circles. Laparotomy group (Lap) versus device-implanted (Dev) group without stimulation. N = 9 mice per group. Student's t-test (two-tailed, unpaired). ns: no significant difference. Error bars represent SEM.

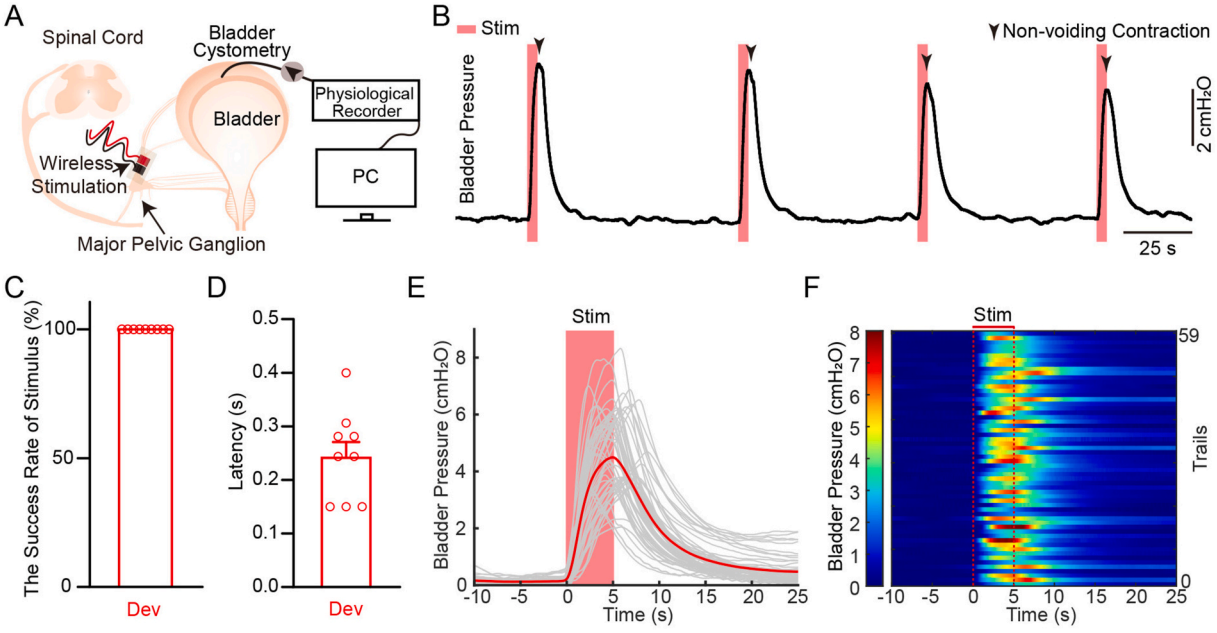

Fig. 3. Examining the Influence of Wireless Electrical Stimulation on Bladder Contraction via the Major Pelvic Ganglion (A) Schematic of the wireless electrical stimulation experiment. Electrical stimulation is targeted at the MPG (Major Pelvic Ganglion), while bladder catheterization and monitoring of bladder pressure are conducted simultaneously. (B) Representative intravesical pressure (IVP) traces during non-continuous transvesical infusion cystometry in device-implanted mice. Non voiding events are denoted with an arrowhead. Stimulation (Stim). (C) Success rate of electrical stimulation at MPG inducing IVP in device-implanted mice (Dev). (D) Quantification of the time interval between the initiation of IVP changes and the onset of electrical stimulation. N = 9 mice. (E–F) Plot of IVP traces aligned to the onset of electrical stimulation. Overlay of all trials in Figure E, Gray traces, individual trials; red, mean. Intravesical pressure data were subjected to Savitzky-Golay filtering in Figure E. Heat maps of individual IVP traces aligned to stimulation onsets in Figure F (n = 59 trials, 9 male mice). Error bars represent the SEM. (For interpretation of the references to colour in this figure legend, the reader is referred to the Web version of this article.)

electrical stimulation parameters on IVP were measured through MPG stimulation (Supplementary Figs. 2a–2f). Representative IVP traces during non-continuous transvesical infusion cystometry in device-implanted mice showed that different stimulation parameters induced changes in IVP. More importantly, the peak pressure values were closely related to the stimulation parameters (Supplementary Figs. 2a–2f). Notably, the device-induced (Dev) IVP did not result in fluid elimination from the urethra (Fig. 3B, 3E and 3F). Additionally, the success rate of wireless electrical stimulation in inducing bladder contraction was 100% (Fig. 3C), with a latency of approximately 0.25 s between the onset of stimulation and the initiation of bladder contraction (Fig. 3D).

Electrical stimulation, known for its safety and reversibility, has been extensively studied and applied in the clinical treatment of LUTD over the past few decades [43,47]. Additionally, prolonged electrical stimulation has been shown to cause no damage to nerves [48]. Here, we further evaluated the long-term effects of electrical stimulation on bladder function. Bladder pressure was monitored during electrical stimulation after varying durations of stimulation (30 times per day for 1 week, 2 weeks, and 3 weeks) (Supplementary Figs. 4a–4c). To prevent muscle adaptation or memory effects due to regular stimulation intervals, we applied electrical stimulation at random intervals. The results showed no significant differences in the latency of detrusor contractions or peak pressure during stimulation after different durations of treatment (Supplementary Figs. 4d and 4e). Additionally, the impact of long-term electrical stimulation on reflexive bladder voiding was assessed. Bladder pressure changes induced by reflexive voiding were monitored during bladder filling before stimulation (Before) and after 3 weeks (Post) of stimulation (Supplementary Figs. 4f and 4g). Compared to the before group, no significant differences were observed in peak bladder pressure or pressure difference during filling (Supplementary Figs. 4h and 4i). Histological analysis of bladder sections stained with H&E revealed no significant differences in bladder wall thickness between mice subjected to 3 weeks of electrical stimulation and laparotomy (Lap) mice. Furthermore, there was no evidence of epithelial inflammation, edema, or capillary congestion (Supplementary Figs. 4j and 4k). In summary, these findings suggest that subcutaneous implantation of an electrical stimulation device targeting the MPG can effectively control bladder contractions in mice. Long-term electrical stimulation reliably induces detrusor contractions without negatively impacting bladder function.

3.4. *Wireless programmable electrical stimulation device control mouse micturition*

To further investigate the feasibility of wireless device stimulation, we implanted the device in the MPG in the abdomen of mice (Supplementary Fig. 3a) with bilateral pudendal nerve transection to simulate sacral nerve stimulation (Fig. 4A). First, we performed urine spot monitoring in mice while stimulating the MPG (Supplementary Videos 1 and 2). Wireless electrical stimulation of the MPG (stimulation frequency: 25 Hz; duration: 5 s; pulse width: 10 ms; pulse interval: 30 ms; stimulation voltage: 1 V) via this device induced micturition in freely moving mice with bilateral pudendal nerve transection (Fig. 4B). Compared with the diameter of urinary spots during micturition in the sham group, the proportion of urinary spots induced by wireless electrical stimulation (Device group) with a diameter >3 cm was 50% (Fig. 4C). To further monitor the effects of wireless electrical stimulation of the MPG on bladder pressure in mice with bilateral pudendal nerve transection, we combined MPG wireless electrical stimulation with cystometry in urethane-anesthetized mice. Wireless electrical stimulation induced urination with a success rate of 100% (Fig. 4E), and the pattern of IVP changes induced by wireless electrical stimulation closely resembled natural reflexive urination (Fig. 4D). The delay between the onset of stimulation and the initiation of bladder contraction was approximately 0.25 s (Fig. 4F). This interval reflects the time required to induce bladder contraction after stimulation, demonstrating that the electrical stimulation method can quickly and efficiently evoke bladder

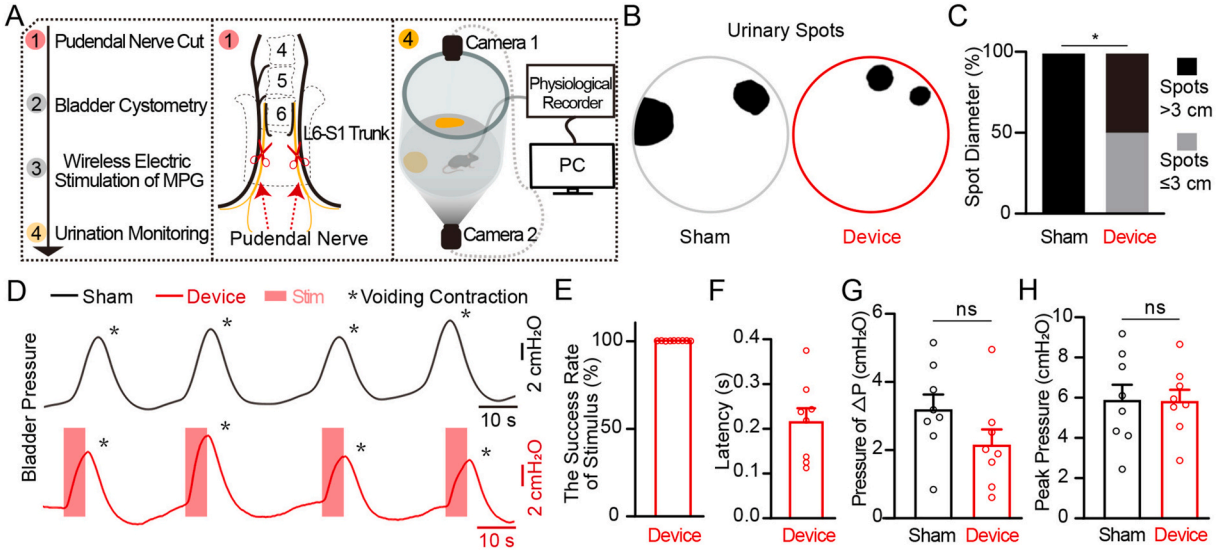

Fig. 4. Effects of Wireless Electrical Stimulation on Bladder Behavior after Bilateral Pudendal Nerve Transection (A) Flowchart of the wireless electrical stimulation experiment. Implantation of wireless electrical stimulation device at the MPG (Major Pelvic Ganglion) is performed in mice after bilateral pudendal nerve transection, while monitoring the mice's urine spots or recording bladder pressure changes after bladder catheterization. (B) Examples of urinary spots of the sham group (Sham) and device-implanted group (Device). The sham group consisted of device-implanted mice without stimulation. (C) Quantification of the diameters of urinary spots in Figure B. (D) Representative intravesical pressure (IVP) traces during continuous transvesical infusion cystometry in device or sham group. The sham group consisted of device-implanted mice but without stimulation, and without pudendal nerve transection. Each voiding event is denoted with an asterisk. Intravesical pressure data was subjected to Savitzky-Golay filtering in Figure D. (E) Success rate of electrical stimulation at MPG inducing IVP in device group. (F) Quantification of the time interval between the initiation of IVP changes and the onset of electrical stimulation. (G) Quantification of the variation in IVP (ΔP). ΔP denotes the difference between threshold pressure (sudden increase in bladder pressure) and end pressure. N = 8 mice for each group. Student's *t*-test (two-tailed, unpaired), ns: no significant difference. (H) Quantification of peak pressure for the sham group and device group. N = 8 mice for each group. Student's *t*-test (two-tailed, unpaired), ns: no significant difference. Error bars represent SEM.

contraction. This process simulates the physiological conduction of nerve impulses through the MPG to the bladder, leading to contractions. These results highlight the immediate effect of electrical stimulation and its efficiency in bladder control. Furthermore, wireless electrical stimulation led to a negative pressure change, allowing urine to flow from the urethra, with a bladder pressure difference of approximately 2 cmH_2O, which was not statistically different from the sham group (Fig. 4G). The peak pressure induced by stimulation was approximately 6 cmH_2O, which was not statistically different from that of the sham group (Fig. 4H). Overall, these findings imply that the wireless device can effectively control micturition in mice with bilateral pudendal nerve transection by stimulating MPG.

4. Discussion

In this study, we present an innovative wireless battery-free device for regulating bladder contractions, aimed at improving electrical stimulation therapy for patients with LUTD. Compared to traditional interventions such as medication and surgery, the method offers several advantages, including reversibility of intervention, miniaturization of the device, real-time adjustment of parameters, and low cost. The stimulation control demonstrated rapid reversibility, with bladder pressure quickly rising during MPG electrical stimulation and promptly decreasing once stimulation ceased (Fig. 3B; Supplementary Figs. 2a, 2c, and 2e). In contrast to the existing active SNM electrical stimulation interventions, this device is designed for wireless power transmission via magnetic induction coupling. This design provides multiple benefits over current treatment methods. Firstly, its miniaturized design eliminates the need for external batteries, weighing less than 0.2 g and with a volume of less than 0.1 cubic centimeters (Fig. 1A–C). This reduction in size and weight allows for minimally invasive procedures and eliminates the need for external connections, thereby simplifying the surgical process and reducing patient discomfort. This represents a significant improvement over previous devices such as Medtronic's Intellis™ System, which, despite being the smallest neural stimulator on the market [17,18], still presents risks of post-implantation infection or displacement and carries a high treatment cost. Furthermore, the device, composed of low-cost diodes and flexible electrodes (Fig. 1A and 1D), is expected to decrease treatment costs and increase patient acceptance of such therapies. Moreover, the wireless stimulator's ability to allow for real-time adjustment of key parameters, such as stimulation voltage, duration, frequency, pulse width, and pulse interval, represents a major technological leap (Fig. 2B and 2C). This level of control and precision is crucial for tailoring treatments to individuals' needs and for optimizing therapeutic outcomes. In summary, the wireless, battery-free device reported in this study offers significant advantages for the electrical stimulation treatment of LUTD. These advantages include minimally invasive procedures, real-time parameter adjustment, and low cost.

The precision of device control is always a concern when it is in use. In fact, the stability of the device output is closely related to animal behavior and the RF antenna. Variations in the height and angle of the device relative to the RF antenna can result in changes in magnetic flux. For more complex applications, addressing the changes in angle and height between the device and the RF antenna caused by movements typically involves increasing magnetic field coverage. This is often achieved by using dual-loop antennas or angled antennas to enhance the stability of energy transmission, accommodating a wider range of device movements [33,49]. However, in the context of electrical stimulation for mouse urination control (Supplementary Videos 1 and 2), the posture of the mice remains fixed during urination, meaning they keep their bodies still. Consequently, the angle and height between the device and the RF antenna remain relatively constant. Therefore, in our study, stable output control of the electrical stimulation was achieved using a single-loop RF antenna.

By targeting the major pelvic ganglion (MPG), the wireless stimulator achieved a 100% success rate in controlling bladder contractions in mice (Fig. 3B and 3C). MPG stimulation in this study is believed to induce excitatory postsynaptic potentials (EPSPs) in the MPG, leading to significant recruitment and release of acetylcholine (ACh) at the synaptic terminals. Upon release, ACh binds to receptors on detrusor muscle cells, triggering depolarization and subsequent calcium ion influx, which in turn initiates detrusor muscle cell contraction, ultimately resulting in overall bladder detrusor contraction [7]. Bladder pressure monitoring showed an increase in intravesical pressure. This suggests that the device has the potential to be a reliable and effective treatment option for patients with refractory UAB or NLUTD, such as that caused by spinal cord injury.

Normal micturition requires coordination between the bladder detrusor and the external urethral sphincter [3]. Although Lee et al. have achieved control of micturition through electrical stimulation of the rat bladder wall [39], numerous studies have indicated limited clinical success with direct bladder wall stimulation. This is due to problems with concomitant sphincter activation (DSD) caused by reflex activity evoked by the activation of pelvic afferents in the bladder [43,50,51]. In our study, when we electrically stimulated the MPG, which directly innervates the bladder muscle, we observed only immediate and time-locked increases in IVP, with no fluid elimination from the urethra (Fig. 3B, 3E and 3F). This observation is consistent with previous research. Therefore, to further validate the efficacy of the device, we used mice in which the pudendal nerve, responsible for innervating the external urethral sphincter, was transected. In this case, electrical stimulation of the MPG successfully induced urine elimination, a procedure analogous to sacral nerve stimulation combined with dorsal rhizotomy (Fig. 4B and 4D). However, the long-term efficacy of the device remains to be evaluated, which is a critical direction for future research. Overall, the development of this wireless stimulator represents a promising therapeutic approach for the treatment of LUTD. This study has addressed the limitations associated with traditional battery-powered electrical stimulators for bladder control. The device's potential for personalized treatment, minimal invasiveness and high therapeutic efficacy make it a valuable addition to the current treatments available for LUTD.

Ethics approval and consent to participate

All experimental manipulations were performed in accordance with the Animal Welfare Guidelines of Third Military Medical University (TMMU) and the National Institutes of Health Guidelines for the Care and Use of Laboratory Animals and were approved by the TMMU Animal Care and Use Committee.

CRediT authorship contribution statement

Jun Li: Writing – original draft, Visualization, Validation, Software, Project administration, Methodology, Investigation, Data curation, Conceptualization. **Guoxian Deng:** Visualization, Validation, Project administration. **Xianping Li:** Visualization, Validation. **Lingxuan Yin:** Validation, Methodology. **Chunhui Yuan:** Validation, Formal analysis. **Wei Shao:** Software. **Xiaowen Xia:** Software. **Junan Yan:** Writing – review & editing, Funding acquisition, Conceptualization. **Jiwei Yao:** Writing – review & editing, Resources, Project administration, Funding acquisition, Conceptualization.

Declaration of competing interest

The authors declare that they have no known competing financial interests or personal relationships that could have appeared to influence the work reported in this paper.

Data availability

Data will be made available on request.

Acknowledgments

This study was supported by grants from the National Natural Science Foundation of China (32100912, 31970946), China Postdoctoral Science Foundation (2021M700602), and Talent Project of Chongqing (4246ZP1252).

Appendix A. Supplementary data

Supplementary data to this article can be found online at https://doi.org/10.1016/j.mtbio.2024.101233.

References

[1] A.M.J. Verstegen, N. Klymko, L. Zhu, J.C. Mathai, R. Kobayashi, A. Venner, R. A. Ross, V.G. VanderHorst, E. Arrigoni, J.C. Geerling, M.L. Zeidel, Non-crh glutamatergic neurons in barrington's nucleus control micturition via glutamatergic afferents from the midbrain and hypothalamus, Curr. Biol. 29 (2019) 2775–2789.e7, https://doi.org/10.1016/j.cub.2019.07.009.

[2] J. Yao, Q. Zhang, X. Liao, Q. Li, S. Liang, X. Li, Y. Zhang, X. Li, H. Wang, H. Qin, M. Wang, J. Li, J. Zhang, W. He, W. Zhang, T. Li, F. Xu, H. Gong, H. Jia, X. Xu, J. Yan, X. Chen, A corticopontine circuit for initiation of urination, Nat. Neurosci. 21 (2018) 1541–1550, https://doi.org/10.1038/s41593-018-0256-4.

[3] J.A. Keller, J. Chen, S. Simpson, E.H.-J. Wang, V. Lilascharoen, O. George, B. K. Lim, L. Stowers, Voluntary urination control by brainstem neurons that relax the urethral sphincter, Nat. Neurosci. 21 (2018) 1229–1238, https://doi.org/10.1038/s41593-018-0204-3.

[4] X.H. Hou, M. Hyun, J. Taranda, K.W. Huang, E. Todd, D. Feng, E. Atwater, D. Croney, M.L. Zeidel, P. Osten, B.L. Sabatini, Central control circuit for context-dependent micturition, Cell 167 (2016) 73–86.e12, https://doi.org/10.1016/j.cell.2016.08.073.

[5] C.J. Fowler, D. Griffiths, W.C. de Groat, The neural control of micturition, Nat. Rev. Neurosci. 9 (2008) 453–466, https://doi.org/10.1038/nrn2401.

[6] J.N. Panicker, C.J. Fowler, T.M. Kessler, Lower urinary tract dysfunction in the neurological patient: clinical assessment and management, Lancet Neurol. 14 (2015) 720–732, https://doi.org/10.1016/S1474-4422(15)00070-8.

[7] W.C. de Groat, D. Griffiths, N. Yoshimura, Neural control of the lower urinary tract, in: R. Terjung (Ed.), Comprehensive Physiology, first ed., Wiley, 2014, pp. 327–396, https://doi.org/10.1002/cphy.c130056.

[8] M.J. Drake, J. Williams, D.A. Bijos, Voiding dysfunction due to detrusor underactivity: an overview, Nat. Rev. Urol. 11 (2014) 454–464, https://doi.org/10.1038/nrurol.2014.156.

[9] H.-C. Kuo, Botulinum A toxin urethral injection for the treatment of lower urinary tract dysfunction, J. Urol. 170 (2003) 1908–1912, https://doi.org/10.1097/01.ju.0000091281.50081.f0.

[10] C. Fontaine, E. Papworth, J. Pascoe, H. Hashim, Update on the management of overactive bladder, Therapeutic Advances in Urology 13 (2021) 175628722110390, https://doi.org/10.1177/17562872211039034.

[11] L. Chen, H. Kuo, Current management of refractory overactive bladder, Low. Urin. Tract. Symptoms 12 (2020) 109–116, https://doi.org/10.1111/luts.12304.

[12] E.I. Kreydin, C.M. Gomes, F. Cruz, Current pharmacotherapy of overactive bladder, Int. Braz J. Urol. 47 (2021) 1091–1107, https://doi.org/10.1590/s1677-5538.ibju.2021.99.12.

[13] J.-J. Wyndaele, The management of neurogenic lower urinary tract dysfunction after spinal cord injury, Nat. Rev. Urol. 13 (2016) 705–714, https://doi.org/10.1038/nrurol.2016.206.

[14] J. Milligan, L.L. Goetz, M.J. Kennelly, A primary care provider's guide to management of neurogenic lower urinary tract dysfunction and urinary tract infection after spinal cord injury, Top. Spinal Cord Inj. Rehabil. 26 (2020) 108–115, https://doi.org/10.46292/sci2602-108.

[15] M. Tutolo, E. Ammirati, J. Heesakkers, T.M. Kessler, K.M. Peters, T. Rashid, K.-D. Sievert, M. Spinelli, G. Novara, F. Van Der Aa, D. De Ridder, Efficacy and safety of sacral and percutaneous tibial neuromodulation in non-neurogenic lower urinary tract dysfunction and chronic pelvic pain: a systematic review of the literature, Eur. Urol. 73 (2018) 406–418, https://doi.org/10.1016/j.eururo.2017.11.002.

[16] T.M. Kessler, D. La Framboise, S. Trelle, C.J. Fowler, G. Kiss, J. Pannek, B. Schurch, K.-D. Sievert, D.S. Engeler, Sacral neuromodulation for neurogenic lower urinary tract dysfunction: systematic review and meta-analysis, Eur. Urol. 58 (2010) 865–874, https://doi.org/10.1016/j.eururo.2010.09.024.

[17] T.M. Kessler, D. La Framboise, S. Trelle, C.J. Fowler, G. Kiss, J. Pannek, B. Schurch, K.-D. Sievert, D.S. Engeler, Sacral neuromodulation for neurogenic lower urinary tract dysfunction: systematic review and meta-analysis, Eur. Urol. 58 (2010) 865–874, https://doi.org/10.1016/j.eururo.2010.09.024.

[18] D.S. Elterman, The novel Axonics® rechargeable sacral neuromodulation system: procedural and technical impressions from an initial North American experience, Neurourol. Urodyn. 37 (2018), https://doi.org/10.1002/nau.23482.

[19] R. Coolen, J. Groen, B. Blok, Electrical Stimulation in the Treatment of Bladder Dysfunction: Technology Update, Medical Devices: Evidence and Research, vol. 12, 2019, pp. 337–345, https://doi.org/10.2147/MDER.S179898.

[20] A.J. Bandodkar, P. Gutruf, J. Choi, K. Lee, Y. Sekine, J.T. Reeder, W.J. Jeang, A. J. Aranyosi, S.P. Lee, J.B. Model, R. Ghaffari, C.-J. Su, J.P. Leshock, T. Ray, A. Verrillo, K. Thomas, V. Krishnamurthi, S. Han, J. Kim, S. Krishnan, T. Hang, J. A. Rogers, Battery-free, skin-interfaced microfluidic/electronic systems for simultaneous electrochemical, colorimetric, and volumetric analysis of sweat, Sci. Adv. 5 (2019) eaav3294, https://doi.org/10.1126/sciadv.aav3294.

[21] H.U. Chung, B.H. Kim, J.Y. Lee, J. Lee, Z. Xie, E.M. Ibler, K. Lee, A. Banks, J. Y. Jeong, J. Kim, C. Ogle, D. Grande, Y. Yu, H. Jang, P. Assem, D. Ryu, J.W. Kwak, M. Namkoong, J.B. Park, Y. Lee, D.H. Kim, A. Ryu, J. Jeong, K. You, B. Ji, Z. Liu, Q. Huo, X. Feng, Y. Deng, Y. Xu, K.-I. Jang, J. Kim, Y. Zhang, R. Ghaffari, C. M. Rand, M. Schau, A. Hamvas, D.E. Weese-Mayer, Y. Huang, S.M. Lee, C.H. Lee, N. R. Shanbhag, A.S. Paller, S. Xu, J.A. Rogers, Binodal, wireless epidermal electronic systems with in-sensor analytics for neonatal intensive care, Science 363 (2019) eaau0780, https://doi.org/10.1126/science.aau0780.

[22] S.M. Won, E. Song, J.T. Reeder, J.A. Rogers, Emerging modalities and implantable Technologies for neuromodulation, Cell 181 (2020) 115–135, https://doi.org/10.1016/j.cell.2020.02.054.

[23] L. Tian, B. Zimmerman, A. Akhtar, K.J. Yu, M. Moore, J. Wu, R.J. Larsen, J.W. Lee, J. Li, Y. Liu, B. Metzger, S. Qu, X. Guo, K.E. Mathewson, J.A. Fan, J. Cornman, M. Fatina, Z. Xie, Y. Ma, J. Zhang, Y. Zhang, F. Dolcos, M. Fabiani, G. Gratton, T. Bretl, L.J. Hargrove, P.V. Braun, Y. Huang, J.A. Rogers, Large-area MRI-compatible epidermal electronic interfaces for prosthetic control and cognitive monitoring, Nat. Biomed. Eng. 3 (2019) 194–205, https://doi.org/10.1038/s41551-019-0347-x.

[24] K. Lee, X. Ni, J.Y. Lee, H. Arafa, D.J. Pe, S. Xu, R. Avila, M. Irie, J.H. Lee, R. L. Easterlin, D.H. Kim, H.U. Chung, O.O. Olabisi, S. Getaneh, E. Chung, M. Hill, J. Bell, H. Jang, C. Liu, J.B. Park, J. Kim, S.B. Kim, S. Mehta, M. Pharr, A. Tzavelis, J.T. Reeder, I. Huang, Y. Deng, Z. Xie, C.R. Davies, Y. Huang, J.A. Rogers, Mechano-acoustic sensing of physiological processes and body motions via a soft wireless device placed at the suprasternal notch, Nat. Biomed. Eng. 4 (2019) 148–158, https://doi.org/10.1038/s41551-019-0480-6.

[25] J.T. Reeder, Y. Xue, D. Franklin, Y. Deng, J. Choi, O. Prado, R. Kim, C. Liu, J. Hanson, J. Ciraldo, A.J. Bandodkar, S. Krishnan, A. Johnson, E. Patnaude, R. Avila, Y. Huang, J.A. Rogers, Resettable skin interfaced microfluidic sweat collection devices with chemesthetic hydration feedback, Nat. Commun. 10 (2019) 5513, https://doi.org/10.1038/s41467-019-13431-8.

[26] X. Yu, Z. Xie, Y. Yu, J. Lee, A. Vazquez-Guardado, H. Luan, J. Ruban, X. Ning, A. Akhtar, D. Li, B. Ji, Y. Liu, R. Sun, J. Cao, Q. Huo, Y. Zhong, C. Lee, S. Kim, P. Gutruf, C. Zhang, Y. Xue, Q. Guo, A. Chempakasseril, P. Tian, W. Lu, J. Jeong, Y. Yu, J. Cornman, C. Tan, B. Kim, K. Lee, X. Feng, Y. Huang, J.A. Rogers, Skin-integrated wireless haptic interfaces for virtual and augmented reality, Nature 575 (2019) 473–479, https://doi.org/10.1038/s41586-019-1687-0.

[27] H.U. Chung, A.Y. Rwei, A. Hourlier-Fargette, S. Xu, K. Lee, E.C. Dunne, Z. Xie, C. Liu, A. Carlini, D.H. Kim, D. Ryu, E. Kulikova, J. Cao, I.C. Odland, K.B. Fields, B. Hopkins, A. Banks, C. Ogle, D. Grande, J.B. Park, J. Kim, M. Irie, H. Jang, J. Lee, Y. Park, J. Kim, H.H. Jo, H. Hahm, R. Avila, Y. Xu, M. Namkoong, J.W. Kwak, E. Suen, M.A. Paulus, R.J. Kim, B.V. Parsons, K.A. Human, S.S. Kim, M. Patel, W. Reuther, H.S. Kim, S.H. Lee, J.D. Leedle, Y. Yun, S. Rigali, T. Son, I. Jung, H. Arafa, V.R. Soundararajan, A. Ollech, A. Shukla, A. Bradley, M. Schau, C. M. Rand, L.E. Marsillio, Z.L. Harris, Y. Huang, A. Hamvas, A.S. Paller, D.E. Weese-Mayer, J.Y. Lee, J.A. Rogers, Skin-interfaced biosensors for advanced wireless physiological monitoring in neonatal and pediatric intensive-care units, Nat Med 26 (2020) 418–429, https://doi.org/10.1038/s41591-020-0792-9.

[28] J.T. Reeder, J. Choi, Y. Xue, P. Gutruf, J. Hanson, M. Liu, T. Ray, A.J. Bandodkar, R. Avila, W. Xia, S. Krishnan, S. Xu, K. Barnes, M. Pahnke, R. Ghaffari, Y. Huang, J. A. Rogers, Waterproof, electronics-enabled, epidermal microfluidic devices for sweat collection, biomarker analysis, and thermography in aquatic settings, Sci. Adv. 5 (2019) eaau6356, https://doi.org/10.1126/sciadv.aau6356.

[29] S.Y. Heo, J. Kim, P. Gutruf, A. Banks, P. Wei, R. Pielak, G. Balooch, Y. Shi, H. Araki, D. Rollo, C. Gaede, M. Patel, J.W. Kwak, A.E. Peña-Alcántara, K.-T. Lee, Y. Yun, J. K. Robinson, S. Xu, J.A. Rogers, Wireless, battery-free, flexible, miniaturized dosimeters monitor exposure to solar radiation and to light for phototherapy, Sci. Transl. Med. 10 (2018) eaau1643, https://doi.org/10.1126/scitranslmed.aau1643.

[30] M. Yuan, Y. Long, T. Liu, J. Liu, S. Qiu, T. Lin, F. Xu, Y. Fang, Soft electronics for advanced infant monitoring, Mater. Today 75 (2024), https://doi.org/10.1016/j.mattod.2024.03.005.

[31] Y. Yang, M. Wu, A. Vázquez-Guardado, A.J. Wegener, J.G. Grajales-Reyes, Y. Deng, T. Wang, R. Avila, J.A. Moreno, S. Minkowicz, V. Dumrongprechachan, J. Lee, S. Zhang, A.A. Legaria, Y. Ma, S. Mehta, D. Franklin, L. Hartman, W. Bai, M. Han, H. Zhao, W. Lu, Y. Yu, X. Sheng, A. Banks, X. Yu, Z.R. Donaldson, R.W. Gereau, C. H. Good, Z. Xie, Y. Huang, Y. Kozorovitskiy, J.A. Rogers, Wireless multilateral devices for optogenetic studies of individual and social behaviors, Nat. Neurosci. 24 (2021) 1035–1045, https://doi.org/10.1038/s41593-021-00849-x.

[32] A.D. Mickle, S.M. Won, K.N. Noh, J. Yoon, K.W. Meacham, Y. Xue, L.A. McIlvried, B.A. Copits, V.K. Samineni, K.E. Crawford, D.H. Kim, P. Srivastava, B.H. Kim, S. Min, Y. Shiuan, Y. Yun, M.A. Payne, J. Zhang, H. Jang, Y. Li, H.H. Lai, Y. Huang, S.-I. Park, R.W. Gereau, J.A. Rogers, A wireless closed-loop system for optogenetic peripheral neuromodulation, Nature 565 (2019) 361–365, https://doi.org/10.1038/s41586-018-0823-6.

[33] G. Shin, A.M. Gomez, R. Al-Hasani, Y.R. Jeong, J. Kim, Z. Xie, A. Banks, S.M. Lee, S. Y. Han, C.J. Yoo, J.-L. Lee, S.H. Lee, J. Kurniawan, J. Tureb, Z. Guo, J. Yoon, S.-I. Park, S.Y. Bang, Y. Nam, M.C. Walicki, V.K. Samineni, A.D. Mickle, K. Lee, S. Y. Heo, J.G. McCall, T. Pan, L. Wang, X. Feng, T. Kim, J.K. Kim, Y. Li, Y. Huang, R. W. Gereau, J.S. Ha, M.R. Bruchas, J.A. Rogers, Flexible near-field wireless optoelectronics as subdermal implants for broad applications in optogenetics, Neuron 93 (2017) 509–521.e3, https://doi.org/10.1016/j.neuron.2016.12.031.

[34] S.I. Park, D.S. Brenner, G. Shin, C.D. Morgan, B.A. Copits, H.U. Chung, M.Y. Pullen, K.N. Noh, S. Davidson, S.J. Oh, J. Yoon, K.-I. Jang, V.K. Samineni, M. Norman, J.

G. Grajales-Reyes, S.K. Vogt, S.S. Sundaram, K.M. Wilson, J.S. Ha, R. Xu, T. Pan, T. Kim, Y. Huang, M.C. Montana, J.P. Golden, M.R. Bruchas, R.W. Gereau, J. A. Rogers, Soft, stretchable, fully implantable miniaturized optoelectronic systems for wireless optogenetics, Nat. Biotechnol. 33 (2015) 1280–1286, https://doi.org/10.1038/nbt.3415.

[35] K.L. Montgomery, A.J. Yeh, J.S. Ho, V. Tsao, S. Mohan Iyer, L. Grosenick, E. A. Ferenczi, Y. Tanabe, K. Deisseroth, S.L. Delp, A.S.Y. Poon, Wirelessly powered, fully internal optogenetics for brain, spinal and peripheral circuits in mice, Nat. Methods 12 (2015) 969–974, https://doi.org/10.1038/nmeth.3536.

[36] T.-M. Jang, J.H. Lee, H. Zhou, J. Joo, B.H. Lim, H. Cheng, S.H. Kim, I.-S. Kang, K.-S. Lee, E. Park, S.-W. Hwang, Expandable and implantable bioelectronic complex for analyzing and regulating real-time activity of the urinary bladder, Sci. Adv. 6 (2020) eabc9675, https://doi.org/10.1126/sciadv.abc9675.

[37] A. Burton, Z. Wang, D. Song, S. Tran, J. Hanna, D. Ahmad, J. Bakall, D. Clausen, J. Anderson, R. Peralta, K. Sandepudi, A. Benedetto, E. Yang, D. Basrai, L.E. Miller, M.C. Tresch, P. Gutruf, Fully implanted battery-free high power platform for chronic spinal and muscular functional electrical stimulation, Nat. Commun. 14 (2023) 7887, https://doi.org/10.1038/s41467-023-43669-2.

[38] S. Lee, H. Wang, W.Y. Xian Peh, T. He, S.-C. Yen, N.V. Thakor, C. Lee, Mechano-neuromodulation of autonomic pelvic nerve for underactive bladder: a triboelectric neurostimulator integrated with flexible neural clip interface, Nano Energy 60 (2019) 449–456, https://doi.org/10.1016/j.nanoen.2019.03.082.

[39] J.H. Lee, T.-M. Jang, J.-W. Shin, B.H. Lim, K. Rajaram, W.B. Han, G.-J. Ko, S. M. Yang, S. Han, D.-J. Kim, H. Kang, J.H. Lim, K.-S. Lee, E. Park, S.-W. Hwang, Wireless, fully implantable and expandable electronic system for bidirectional electrical neuromodulation of the urinary bladder, ACS Nano 17 (2023) 8511–8520, https://doi.org/10.1021/acsnano.3c00755.

[40] J. Yao, Q. Li, X. Li, H. Qin, S. Liang, X. Liao, X. Chen, W. Li, J. Yan, Simultaneous measurement of neuronal activity in the pontine micturition center and cystometry in freely moving mice, Front. Neurosci. 13 (2019) 663, https://doi.org/10.3389/fnins.2019.00663.

[41] G. Yao, L. Kang, J. Li, Y. Long, H. Wei, C.A. Ferreira, J.J. Jeffery, Y. Lin, W. Cai, X. Wang, Effective weight control via an implanted self-powered vagus nerve stimulation device, Nat. Commun. 9 (2018) 5349, https://doi.org/10.1038/s41467-018-07764-z.

[42] S. Lee, H. Wang, W.Y.X. Peh, N.V. Thakor, S.-C. Yen, C. Lee, Direct stimulation of bladder pelvic nerve using battery-free neural clip interface, in: 2019 9th International IEEE/EMBS Conference on Neural Engineering (NER), IEEE, San Francisco, CA, USA, 2019, pp. 706–709, https://doi.org/10.1109/NER.2019.8716975.

[43] M.J. McGee, C.L. Amundsen, W.M. Grill, Electrical stimulation for the treatment of lower urinary tract dysfunction after spinal cord injury, J. Spinal Cord Med 38 (2015) 135–146, https://doi.org/10.1179/2045772314Y.0000000299.

[44] R.A. Gaunt, A. Prochazka, Control of urinary bladder function with devices: successes and failures, in: Progress in Brain Research, Elsevier, 2006, pp. 163–194, https://doi.org/10.1016/S0079-6123(05)52011-9.

[45] M.M. Bertrand, J.R. Keast, Dissection of pelvic autonomic ganglia and associated nerves in male and female rats, J. Visualized Exp. (2020) 60904, https://doi.org/10.3791/60904.

[46] M.F. Barbe, S.M. Gomez-Amaya, D.M. Salvadeo, N.S. Lamarre, E. Tiwari, S. Cook, C.P. Glair, D.H. Jang, R.M. Ragheb, A. Sheth, A.S. Braverman, M.R. Ruggieri, Clarification of the innervation of the bladder, external urethral sphincter and clitoris: a neuronal tracing study in female mongrel hound dogs: genitourinary structure innervation in dogs, Anat. Rec. 301 (2018) 1426–1441, https://doi.org/10.1002/ar.23808.

[47] P.E.V. Van Kerrebroeck, The role of electrical stimulation in voiding dysfunction, Eur. Urol. 34 (1998) 27–30, https://doi.org/10.1159/000052272.

[48] P. Yan, X. Yang, X. Yang, W. Zheng, Y. Tan, Prolonged electrical stimulation causes no damage to sacral nerve roots in rabbits, Neural Regen Res 9 (2014) 1217, https://doi.org/10.4103/1673-5374.135327.

[49] A. Burton, S.M. Won, A.K. Sohrabi, T. Stuart, A. Amirhossein, J.U. Kim, Y. Park, A. Gabros, J.A. Rogers, F. Vitale, A.G. Richardson, P. Gutruf, Wireless, battery-free, and fully implantable electrical neurostimulation in freely moving rodents, Microsyst Nanoeng 7 (2021) 62, https://doi.org/10.1038/s41378-021-00294-7.

[50] C.C. Stenberg, H.W. Burnette, R.C. Bunts, Electrical stimulation of human neurogenic bladders: experience with 4 patients, J. Urol. 97 (1967) 79–84, https://doi.org/10.1016/S0022-5347(17)62983-5.

[51] T. Hald, W. Meier, A. Khalili, G. Agrawal, J.G. Benton, A. Kantrowitz, Clinical experience with a radio-linked bladder stimulator, J. Urol. 97 (1967) 73–78, https://doi.org/10.1016/S0022-5347(17)62982-3.